Journal of Physics: Conference Series **505** (2014) 012009 doi:10.1088/1742-6596/505/1/012009

Defects in nitride-based semiconductors probed by positron annihilation

A Uedono[1], M Sumiya[2], S Ishibashi[3], N Oshima[4] and R Suzuki[4]

[1] Division of Applied Physics, Faculty of Pure and Applied Science, University of Tsukuba, Tsukuba, Ibaraki 305-8573, Japan
[2] Wide Bandgap Material Group, National Institute for Materials Science, Tsukuba, Ibaraki 305-0044, Japan
[3] Nanosystem Research Institute (NRI) "RICS", National Institute of Advanced Industrial Science and Technology (AIST), Tsukuba, Ibaraki 305-8568, Japan
[4] Research Institute of Instrumentation Frontier, National Institute of Advanced Industrial Science and Technology, Tsukuba, Ibaraki, 305-8568, Japan

E-mail: uedono.akira.gb@u.tsukuba.ac.jp

Abstract. Point defects in $In_xGa_{1-x}N$ grown by metal organic chemical vapor deposition were studied by a monoenergetic positron beam. Measurements of Doppler broadening spectra of the annihilation radiation as a function of incident positron energy for $In_xGa_{1-x}N$ (x = 0.08 and 0.14) showed that vacancy-type defects were introduced with increasing InN composition. From comparisons between coincidence Doppler broadening spectra and the results calculated using the projector augmented-wave method, the major defect species was identified as the complexes between a cation vacancy and nitride vacancies. The concentration of the defects was found to be suppressed by Mg doping. An effect of Mg-doping on the positron diffusion properties in GaN and InN was also discussed. The momentum distribution of electrons at the $In_xGa_{1-x}N$/GaN interface was close to that in defect-free GaN or $In_xGa_{1-x}N$, which was attributed to the localization of positrons at the interface due to the electric field caused by polarizations.

1. Introduction

Growth techniques of GaN and Ga-rich $In_xGa_{1-x}N$ have been extensively studied for the past two decades, and this has led to the realization of present GaN-based solid state lighting technologies [1,2]. The $In_xGa_{1-x}N$ material system has also attracted great research interest for use as high-efficiency thin-film photovoltaic device materials [3] because of its potential in controlling the band gaps spanning from 0.65 eV to 3.43 eV, which can cover the wavelength from infrared to ultraviolet regions. The theoretical conversion efficiency of the solar cell using $In_xGa_{1-x}N$ has been reported to be greater than 60% [4]. The efficiency of solar cells using $In_xGa_{1-x}N$/GaN multilayers, however, has been reported to be lower than the theoretical value. The origin of the degradation has been explained by low $In_xGa_{1-x}N$ crystal quality which mainly due to the difficulty of its epitaxial growth. This is mainly associated with large differences in the growth temperatures, equilibrium vapor pressures, and lattice constants of InN and GaN. As a result, the film growth process gives rise to unusually high strain and high defect densities. Dislocations and stacking faults, misorientations, residual strains, and phase separations of $In_xGa_{1-x}N$ have been studied [5], but knowledge regarding point-defects, such as monovacancies and vacancy composites, is also crucial to improve the conversion efficiency. Positron annihilation is a powerful

technique for evaluating vacancy-type defects in semiconductors [6], and the defects in group-III nitrides have been investigated using this method [7-9]. In the present study, we have used a monoenergetic positron beam to probe native vacancies in undoped and Mg-doped $In_xGa_{1-x}N$ grown by metal organic chemical vapor deposition (MOCVD).

2. Experiment

The samples investigated were $In_xGa_{1-x}N$ (x = 0.08 and 0.14) grown using MOCVD. The growth method and the optical properties of the samples are described elsewhere [10,11]. 1.4-μm-thick GaN films (+c-face) were grown on sapphire substrates at 1000°C with buffer layers, and then 300-nm-thick $In_xGa_{1-x}N$ films were grown. For $In_{0.14}Ga_{0.86}N$, the film was deposited on Mg-doped GaN(120 nm)/GaN/sapphire substrate. The growth temperatures of the $In_xGa_{1-x}N$ layers were 790-800°C, respectively. The electron and hole concentrations of undoped and Mg-doped $In_{0.08}Ga_{0.92}N$ were $n_e = 5\times10^{17}$ cm^{-3} and $n_p = 5\times10^{18}$ cm^{-3}, respectively. InN and GaN grown by MOCVD and hydride vapor phase epitaxy (HVPE) were also studied [12,13].

With a monoenergetic positron beam, the Doppler broadening spectra of the annihilation radiation were measured as a function of the incident positron energy E. The low-momentum part of the spectra was characterized by the S parameter, defined as the number of annihilation events over the energy range of 511 keV ± ΔE_γ (where ΔE_γ = 0.76 keV) around the centre of the peak, and the high-momentum part was characterized using the W parameters, defined as the annihilation events in the range of 3.4 keV ≤ $|\Delta E_\gamma|$ ≤ 6.8 keV. The relationship between S and E was analysed by VEPFIT [14].

Doppler broadening spectra corresponding to the annihilation of positrons were theoretically calculated using QMAS (Quantum MAterials Simulator) code, which uses valence-electron wavefunctions determined by the projector augmented-wave (PAW) method [15]. Details of the calculation method and its application to group-III nitrides are described elsewhere [11-13]. The structural optimization was done for a cell containing about 128 atoms by means of *ab initio* quenched molecular dynamics. For $In_{0.5}Ga_{0.5}N$, the initial bulk structure containing 128 atoms has been generated by means of the special-quasirandom-structure (SQS) approach [16]. The simulation was also perfumed for ordered $In_{0.5}Ga_{0.5}N$, where In- and Ga-faces were assumed to locate in c-faces alternately.

3. Results and Discussion

The S values of HVPE-GaN and Mg-doped GaN before and after annealing as a function of E are shown in Fig. 1. The mean implantation depth of positrons is shown on the upper horizontal axis. For HVPE-GaN, the S value saturated at E > 20 keV, suggesting that almost all positrons annihilate in the bulk in this energy range. The solid curve is a fit to the experimental data, and the diffusion length of positrons L_d was obtained as 72±1 nm. The derived value is the typical one for defect-free GaN [11-13]. For Mg-doped GaN after annealing, the S value near the surface (< 1 keV) decreased rapidly with increasing E. For this sample, the L_d value was derived as 2.3±0.1 nm. This very short diffusion length indicates the suppression of thermalized positrons diffusing toward the surface. A schematic of the band structure for p-type GaN is shown as an inset of Fig. 1. Because of the electric field caused by the band bending, the positrons implanted into the depletion region are dragged toward the inside of the sample, and this decreases the L_d value for p-GaN after annealing.

For p-GaN before annealing, the S values at $E \approx 2$ keV were almost the same as those after annealing; above this energy, however, they increased with increasing E (<12 keV), suggesting the trapping of positrons by vacancy-type defects. When the Fermi level position inside the sample was higher than that near the surface, the diffusion of positrons toward the surface would be enhanced. According to this model, the region sampled by the positrons was divided into three blocks; the first and second blocks respectively correspond to the positron annihilation in the Mg-doped layer, and the third block corresponds to that in the Si-doped layer. The derived S values for the first and second layers were close to the S values at E = 2 keV and 12 keV, respectively. The interface between the first and second layers was obtained as 6.4±0.4 nm. The L_d value in the first layer was fixed to the value for the sample after

annealing, and that in the second layer was derived as 127±5 nm. The long diffusion length of positrons in the second layer can be attributed to the enhanced diffusion toward the surface due to the band structure. The *S* value for the first layer was close to that for the sample after annealing, suggesting that the vacancy concentration in the subsurface region (<6 nm) were close to those in the film after annealing. The phenomena observed for the sample before annealing can be attributed to the partial activation of Mg in the subsurface region. Mg is known to segregate on the growth surface of GaN. Thus, because of a combination between the high Mg concentration and an enhanced reaction between Mg and vacancies at the surface, the Fermi level position in the subsurface region could decrease without annealing.

Figure 2 shows the *S*–*E* curves for undoped InN and Mg-doped InN (p-InN, [Mg] = 3.1×10^{19} cm^{-3}) after annealing, where the activation of Mg in p-InN was confirmed using electrolyte-based capacitance-voltage analysis[12]. For the undoped sample, the L_d value was derived as 34±4nm, and this short diffusion length is considered to be related to the surface band bending for InN [17]. The *S*–*E* curve for p-InN can be fitted using the model applied to p-GaN before annealing. The width of the first region and the L_d value in the second block were obtained as 70±7 nm and 127±8 nm, respectively. Thus, a similar band structure discussed for p-type GaN before annealing is expected for p-InN. Because of the electron accumulation at the surface of InN, the confirmation of carrier species in InN is difficult [17]. The present results suggests that the analysis of the *S*–*E* curve can provide useful information about the band structure near the surface.

Figure 3 shows undoped and Mg-doped $In_xGa_{1-x}N$ as a function of incident positron energy *E*. For Mg:$In_{0.08}Ga_{0.92}N$, the *S* value near the surface decreased rapidly with increasing *E*. This is the typical behavior of *S* for *p*-type GaN and InN, and was attributed to the suppression of the positron diffusion toward the surface due to the band bending near the surface. For $In_{0.14}Ga_{0.86}N$, the *S* value was almost flat at *E* = 1-3 keV, which suggests that almost all positrons annihilated in the $In_{0.14}Ga_{0.86}N$ layer without diffusing back to the surface. For all samples, the dips in the *S*–*E* curves were observed at *E* = 10-15 keV, which can be attributed to the annihilation of positrons near the $In_xGa_{1-x}N$/GaN interface.

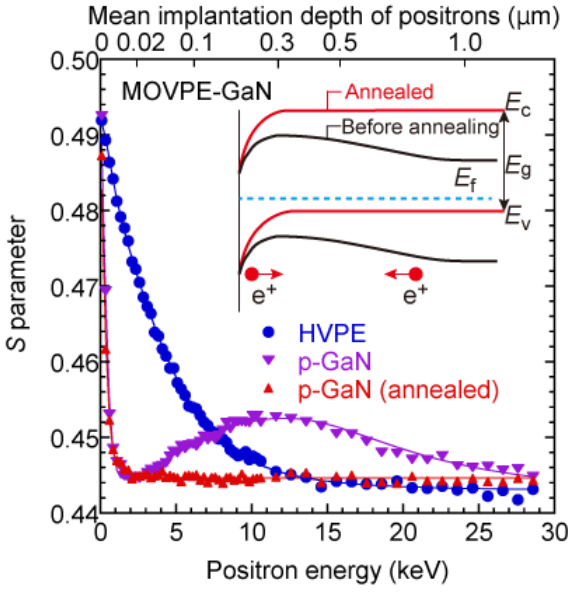

Figure 1. *S* as a function of incident positron energy *E* for undoped HVPE-GaN, Mg-doped GaN (p-GaN) before and after annealing. The solid curves are fits to the experimental data. An inset shows a schematic viewgraph for the band structure for *p*-type GaN.

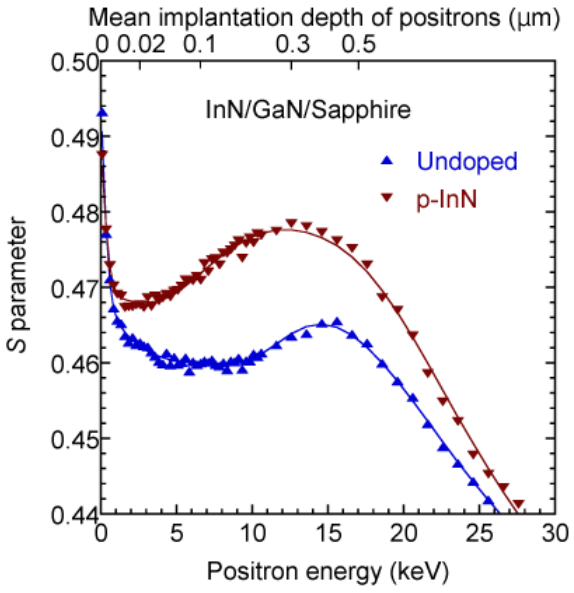

Figure 2. *S* parameters as a function of *E* for undoped and Mg-doped InN (p-InN) after activation of Mg.

Annihilation characteristics of positrons in layered structures can be discussed by graphical analysis of the relationship between the *S* and *W* parameters. Figure 4 shows the *S*–*W* relationship for $In_{0.14}Ga_{0.86}N$, $In_{0.08}Ga_{0.92}N$, and Mg:$In_{0.08}Ga_{0.92}N$. The (*S*,*W*) value for HVPE-GaN (defect-free GaN) is also shown. Arrows show directions of the increase of *E*. For Mg:$In_{0.08}Ga_{0.92}N$, the (*S*,*W*) trajectory can be represented by a straight line [an identical line was also shown in Fig. 4(a) and (b)]. The value approached the defect-free (*S*,*W*) for GaN with increasing *E* ($E \leq 10$ keV). For $In_{0.14}Ga_{0.86}N$, although the (*S*,*W*) value saturated at *E* = 2.9-5.4 keV (corresponding (*S*,*W*) value was shown in dotted lines), above *E* = 5.9 keV, it started to approach the defect-free (*S*,*W*) value. For undoped $In_{0.08}Ga_{0.92}N$, although no clear indication of the annihilation of positrons in the $In_{0.08}Ga_{0.92}N$ layer observed in the *S*–*E* curve, the deviation from the line was observed in the *S*–*W* plot. This suggests that positrons implanted into the $In_xGa_{1-x}N$ layer were under strong influence of the $In_xGa_{1-x}N$/GaN interface. Because the (*S*,*W*) value tend to approach the value for HVPE-GaN, the momentum distribution of electrons near the $In_xGa_{1-x}N$/GaN interface is considered to be close to that for defect free $In_xGa_{1-x}N$ or GaN.

The *S*–*E* curves for $In_xGa_{1-x}N$/GaN were fitted, and the region sampled by the positrons was divided into four blocks; they respectively correspond to the positron annihilation in the $In_xGa_{1-x}N$ layer, the $In_xGa_{1-x}N$/GaN interface, the GaN layer, and the sapphire substrate. The widths of the blocks and the corresponding *S* values were determined by the fitting. The derived depth distributions of *S* are shown

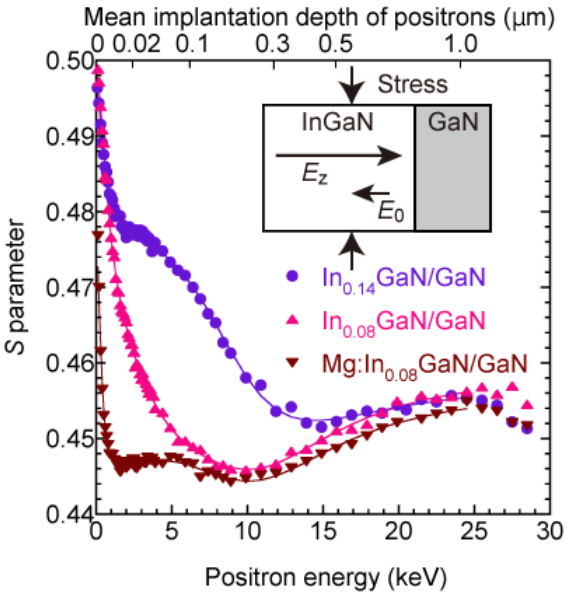

Figure 3. *S* parameters as a function of *E* for undoped In_xGaN_{1-x} (x=0.08 and 0.14) and Mg-doped $In_{0.08}Ga_{0.92}N$. Dips at *E* = 9-15 keV in the curves were attributed to the annihilation of positrons at the In_xGaN_{1-x}/GaN interface. An inset shows the piezoelectric field E_z and the electric field generated from the spontaneous polarization E_0.

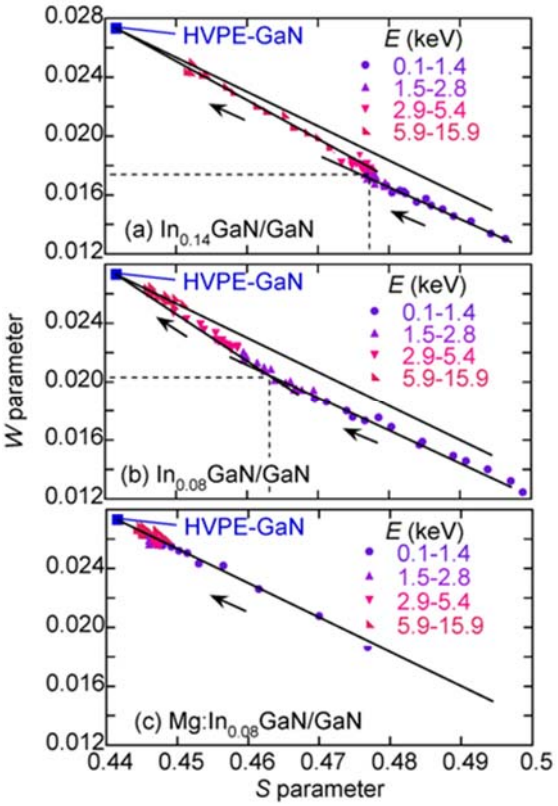

Figure 4. Relationships between *S* and *W* for (a) $In_{0.14}Ga_{0.86}N$, (b) $In_{0.08}Ga_{0.92}N$, and (b) Mg-doped $In_{0.08}Ga_{0.92}N$. The (*S*,*W*) values for HVPE-GaN (defect-free) is also shown. Arrows show the increase in the incident energy of positrons.

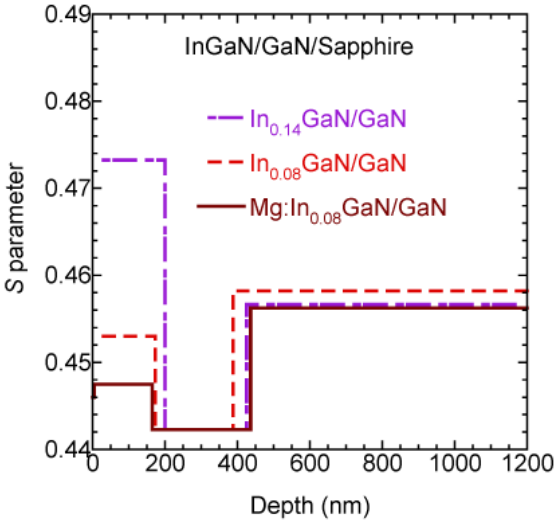

Figure 5. Depth distributions of S for undoped $In_xGa_{1-x}N$ (x = 0.08 and 0.14) and Mg-doped $In_{0.08}Ga_{0.92}N$ derived from the fitting (Fig. 3).

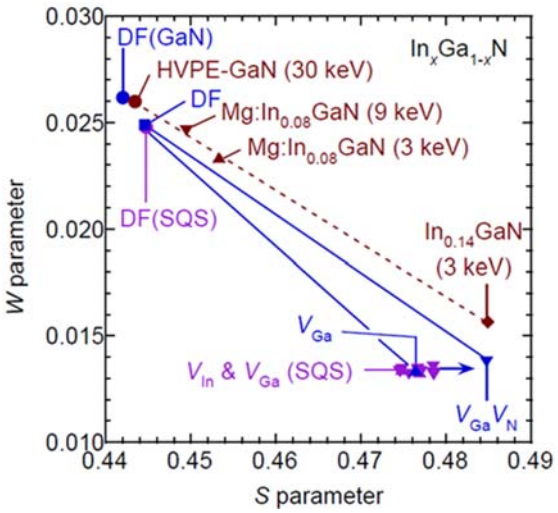

Figure 6. (S,W) values (blue) corresponding to the annihilation of positrons in the delocalized state (defect-free: DF) and that of positrons trapped by V_{Ga} as calculated for $In_{0.125}Ga_{0.875}N$. The result for DF-GaN is also shown. Arrows show the effect of V_N coupled with V_{Ga}. The (S,W) values for $In_{0.14}Ga_{0.86}N$, Mg-doped $In_{0.08}Ga_{0.92}N$, and HVPE-GaN are also shown.

in Fig. 5. For all samples, although the second block represents the $In_xGa_{1-x}N$/GaN interface, their widths were obtained as about 200 nm. Makkonen *et al*. [9] reported the localization of positrons at the InN/GaN interface due to the built-in electric field caused by the piezoelectric effect. Because this effect was not included in the fitting model, the accumulation of positrons near the interface appeared as the wide width of the second block. Because a compressive stress is introduced in the $In_xGa_{1-x}N$ layer grown on the +c-plane GaN template, the positrons in the layer are dragged toward the interface by the piezoelectric field E_z, where the spontaneous electric field E_0 is far smaller than E_z (inset of Fig. 3). This is the major cause of the lack of clear signals for the positron annihilation in the $In_{0.08}Ga_{0.92}N$ layer.

Figure 6 shows the (S,W) values calculated from the coincidence Doppler broadening spectra using the PAW method. The values correspond to the annihilation of positrons in the delocalized state (defect-free: DF) in ordered $In_{0.125}Ga_{0.875}N$ and those of positrons trapped by Ga-vacancy V_{Ga} and divacancy ($V_{Ga}V_N$) (blue symbol) are shown. The result for DF-GaN is also shown. Arrows show the effect of N-vacancy V_N coupled with V_{Ga}. The (S,W) values calculated using SQS for DF-$In_{0.125}Ga_{0.875}N$ and cation vacancies are also shown. The (S,W) values calculated using the ordered structure and SQS are close to each other, suggesting that the (S,W) values calculated using ordered-$In_{0.125}Ga_{0.875}N$ can be used to compare with experimentally obtained values.

Using the coincidence system, the (S,W) values were measured at E = 3 keV for $In_{0.14}Ga_{0.86}N$, at E = 3 and 9 keV for Mg:$In_{0.08}Ga_{0.92}N$, and at E = 30 keV for HVPE-GaN. For $In_{0.14}Ga_{0.86}N$, the obtained value is located on the right side of the line connecting the values of the defect-free and $V_{Ga}V_N$. Because the formation of vacancy complexes with V_N causes a rightward shift in the S–W plot, the major trapping center of positrons can be determined as complexes between a cation vacancy and V_Ns. For Mg:$In_{0.08}Ga_{0.92}N$, the measured (S,W) values are located on the line connecting the values of $In_{0.14}Ga_{0.86}N$ and HVPE-GaN. Thus, the major defect species is expected to be the same as that for $In_{0.14}Ga_{0.86}N$, but their concentration was suppressed by Mg-doping.

Using first-principles calculation [18], it was reported that the formation energy of V_N decreased as the number of In adjacent to V_N increased. Thus, both the bond-length/angle distortions and the decrease

in the formation energy of V_N are expected to promote the introduction of V_N with increasing InN content. Although positrons are not trapped by isolated V_N, some of them preferentially couple with cation vacancies and form stable complexes. Thus, we can conclude that the observed behaviour of defects in in $In_xGa_{1-x}N$ is considered to be the introduction of V_N and related formation of cation-vacancy-V_N complexes.

4. Summary

We studied vacancy-type defects in $In_xGa_{1-x}N$ grown by MOCVD using a monoenergetic positron beam. The major defect species in the $In_xGa_{1-x}N$ film was identified as cation vacancies coupled with V_Ns, and their concentration increased with increasing InN content. The defect concentration, however, was decreased by Mg-doping. The intrinsic (*S*,*W*) value corresponding to the annihilation of positrons at the $In_xGa_{1-x}N$/GaN interface was close to that for defect-free GaN or $In_xGa_{1-x}N$, suggesting the localization of positrons at the interface due to the piezoelectric field. From the measurements of Mg-doped InN, $In_xGa_{1-x}N$, and GaN, it was found that the diffusion property of positrons is sensitive to variation in the band structures in the subsurface region. We have shown that the positron annihilation parameters are sensitive to vacancy-type defects in $In_xGa_{1-x}N$ films, meaning that this technique can be a useful tool for evaluating $In_xGa_{1-x}N$-based devices.

References

[1] Nakamura S and Chichibu S F 2000 *Introduction to Nitride Semiconductor Blue Lasers and Light-Emitting Diodes* (London: Taylor and Francis)
[2] Akasaki I and Amano H 2006 *Jpn. J. Appl. Phys.* **45** 9001
[3] Wu J, Walukiewicz W, Yu K M, Shan W, Ager III J W, Haller E E, Lu H, Schaff W J, Metzger W K and Kurtz S 2003 *J. Appl. Phys.* **94**, 3967
[4] Devos A 1992 *Endoreversible Thermodynamics of Solar Energy Conversion* (New York: Oxford University Press).
[5] Wu J 2009 *J. Appl. Phys.* **106** 011101
[6] Krause-Rehberg R and Leipner H S 1999 *Positron Annihilation in Semiconductors, Solid-State Sciences* (Berlin: Springer-Verlag)
[7] Saarinen K, Laine T, Kuisma S, Nissilä J, Hautojärvi P, Dobrzynski L, Baranowski J M, Pakula K, Stepniewski R, Wojdak M, Wysmolek A, Suski T, Leszczynski M, Grzegory I and Porowski S, 1997 *Phys. Rev. Lett.* **79** 3030
[8] Tuomisto F, Pelli A, Yu K M, Walukiewicz W, Schaff W J 2007 *Phys. Rev. B* **75** 193201
[9] Makkonen I, Snicker A, Puska M J, Mäki J-M and Tuomisto F 2010 *Phys. Rev. B* **82** 041307(R)
[10] Sang L, Liao M, Ikeda N, Koide Y and Sumiya M 2011 *Appl. Phys. Lett.* **99** 161109
[11] Uedono A, Tsutsui T, Watanabe T, Kimura S, Zhang Y, Lozac'h M, Sang L W, Ishibashi S and Sumiya M 2013 *J. Appl. Phys.* **113**, 123502
[12] Uedono A, Nakamori H, Narita K, Suzuki J, Wang X, Che S-B, Ishitani Y, Yoshikawa A and Ishibashi S 2009 *J. Appl. Phys.* **105** 054507
[13] Uedono A, Ishibashi S, Tenjinbayashi K, Tsutsui T, Nakahara K, Takamizu D and Chichibu S F 2012 *J. Appl. Phys.* **111** 014508
[14] Van Veen A, Schut H, De Vries J, Hakvoort R A and Ijpma M R 1990 *AIP Conf. Proc.* **218** 171
[15] Ishibashi S 2004 Materials Science Forum **445-446** 401. Up-to-date information of QMAS is reported in http://qmas.jp/.
[16] Zunger A, Wei S-H, Ferreira L G and Bernard J E 1990 *Phys. Rev. Lett.* **65** 353
[17] Yoshikawa A, Wang X Q, Ishitani Y and Uedono A 2010 *Physica Status Solidi A* **207** 1011
[18] Obata T, Iwata J, Shiraishi K and Oshiyama A, 2009 *J. Crystal Growth* **311** 2772